Cold dust in late-type Virgo Cluster galaxies

Cristina C. Popescu[1,2]

*The Observatories of the Carnegie Institution of Washington, 813 Santa Barbara Str.,
Pasadena, 91101 California, USA*

Richard J. Tuffs, Heinrich J. Völk

Max Planck Institut für Kernphysik, Saupfercheckweg 1, 69117 Heidelberg, Germany

Daniele Pierini

The University of Toledo, Toledo, Ohio 43606-3390, USA

Barry F. Madore[3]

*NASA/IPAC Extragalactic Database, 770 S. Wilson Avenue, Pasadena, California 91125,
USA*

ABSTRACT

We have statistically analyzed the spatially integrated far-infrared (FIR) emissions of the complete volume- and luminosity-limited sample of late-type (later than S0) Virgo cluster galaxies measured using the Infrared Space Observatory (ISO) by Tuffs et al. (2002) in bands centered on 60, 100 & $170\,\mu$m. 30 out of 38 galaxies detected at all three wavelengths contain a cold dust emission component, present within all morphological types of late-type systems ranging from early giant spirals to Blue Compact Dwarfs (BCDs), and which could not have been recognized by IRAS. We fitted the data with a superposition of two modified grey-body functions, physically identified with a localized warm dust emission component associated with HII regions (whose temperature was constrained to be $47\,$K), and a diffuse emission component of cold dust. The cold dust temperatures were found to be broadly distributed, with a median of $18\,$K,

[1]Max Planck Institut für Astronomie, Königstuhl 17, 69117 Heidelberg, Germany

[2]Research Associate, The Astronomical Institute of the Romanian Academy, Str. Cuţitul de Argint 5, Bucharest, Romania

[3]The Observatories of the Carnegie Institution of Washington, 813 Santa Barbara Str., Pasadena, 91101 California, USA

some $8 - 10\,\mathrm{K}$ lower than would have been predicted from IRAS. The derived total dust masses are correspondingly increased by factors of typically $6 - 13$. A good linear correlation is found between the "warm FIR" luminosities and the Hα equivalent widths (EW), supporting the assumptions of our constrained spectral energy distribution (SED) fit procedure. We also found a good non-linear correlation between the "cold FIR" luminosities and the Hα EWs, consistent with the prediction of Popescu et al. (2000) that the FIR-submm emission should mainly be due to diffuse non-ionizing UV photons. Both the "warm" and the "cold" FIR luminosity components are non-linearly correlated with the (predominantly non-thermal) radio luminosities. There is a tendency for the temperatures of the cold dust component to become colder, and for the cold dust surface densities (normalized to optical area) to increase for later morphological types. A particularly significant result concerns the low dust temperatures (ranging down to less than $10\,\mathrm{K}$) and large dust masses associated with the Im and BCD galaxies in our sample. We propose two scenarios to account for the FIR characteristics of these systems.

Subject headings: galaxies: clusters: individual (Virgo cluster)—galaxies: dwarf—galaxies: ISM—galaxies: spiral—galaxies: statistics—infrared: galaxies

1. Introduction

IRAS observations led to the belief that dust emission in normal galaxies comes from $\sim 30\,\mathrm{K}$ dust grains with a total gas-to-dust mass ratio of $\sim 10^3$ (e.g. Devereux & Young 1990). This is about one order of magnitude greater than the gas-to-dust mass ratio our Galaxy, a discrepancy which suggested that most of the dust in late-type galaxies had in fact been "overlooked" by IRAS. Indeed, one obvious bias of IRAS studies in general is the lack of spectral coverage longwards of the $100\,\mu\mathrm{m}$ filter and the three times brighter sensitivity limit in this band compared to the IRAS $60\,\mu\mathrm{m}$ band. This might translate into a bias against the detection of cold dust with temperatures colder than $30\,\mathrm{K}$.

The first observations suggesting the existence of a cold dust component in galaxies were made at sub-millimeter (sub-mm) wavelengths by Chini et al. (1986) using the $3\,\mathrm{m}$ IRTF (Infrared Telescope Facility) and the UH $88''$ telescope (University of Hawaii). The strong sub-mm emission found in all the observed galaxies could not be accounted for by dust emitting at a uniform temperature and the FIR spectra were interpreted in terms of two dust components of about 16 and $53\,\mathrm{K}$. This interpretation suggested that the peak of the FIR emission should be at wavelengths between 100 and $200\,\mu\mathrm{m}$. Subsequent sub-mm

observations done with the 30 m IRAM (Pico Veleta) telescope also suggested the presence of a cold dust component in individual nearby galaxies: NGC 891 (Guélin et al. 1993), NGC 3627 (Sievers et al. 1994), NGC 4631 (Braine et al. 1995), M 51 (Guélin et al. 1995), NGC 4565 (Neininger et al. 1996), NGC 3079 (Braine et al. 1997), NGC 5907 (Dumke et al. 1997). The enhanced sensitivity and overall efficiency improvement of the SCUBA sub-mm array at the JCMT (James Clerk Maxwell Telescope) extended our knowledge of the quantity of cold dust by probing both more "quiescent" galaxies and also by mapping its distribution with higher resolution (Alton et al. 1998a, Israel et al. 1999, Bianchi et al. 2000b, Alton et al. 2001). However, none of these observations directly observed the spectral peak of the FIR emission and thus did not unambiguously distinguish between the two dust components. Observations at 160 and 200 μm were until recently available only for a few bright objects and were performed with the KAO (NASA-Kuiper Airborne Observatory)(e.g. Engargiola 1991).

The ISOPHOT instrument (Lemke et al. 1996) on board the ISO satellite (Kessler et al. 1996) extended for the first time the wavelength coverage beyond that of IRAS, to 240 μm, with superior intrinsic sensitivity, and the availability of longer integration times than were possible with IRAS. ISO was thus capable to cover the peak in energy distribution νS_ν for normal galaxies, detecting discrete sources at least 10 times fainter than IRAS at 60 and 100 μm. First results from ISOPHOT have indeed confirmed the existence of a cold dust component in several nearby normal galaxies: NGC 6946 (Tuffs et al. 1996), M 31 (Haas et al. 1998), or on small samples: Krügel et al. (1998), Siebenmorgen, Krügel & Chini (1999),Contursi et al. (2001). First results from the ISO LWS (Long Wavelength Spectrograph) (Trewhella et al. 2000) are also consistent with the existence of cold dust in normal galaxies. The sample of compact sources with galaxy associations from the ISOPHOT 170 μm serendipity survey (Stickel et al. 2000) presents statistical evidence for a cold dust component, but the sample was obviously biased towards FIR luminous systems, with uncertain transient corrections in the observations.

In this paper we present statistically significant evidence for the existence of a cold dust component in all galaxies later than S0, i.e. spirals, irregulars and Blue Compact Dwarfs (BCDs). This result comes from our analysis of a complete volume- and luminosity-limited sample of late-type Virgo Cluster galaxies observed by Tuffs et al. (2002) with the ISOPHOT instrument. Our sample is intended to give a more representative statistical analysis of the cold dust component, for a full range in morphological type, and to reach fainter detection limits than previously available. In addition, we present our analysis on data which are for the first time corrected from the transient effects of the detectors, allowing a quantitative and comprehensive evaluation of the cold dust on a relatively deep and unbiased sample.

A main goal for our study is the detailed knowledge of the shape of the FIR SED in galaxies, as well as the distribution and morphology of the cold dust. This is required for understanding the energy budget in galaxies and for modeling the SED over the whole wavelength range. Dust grains can be considered as test particles for the intrinsic radiation fields in galaxies. Therefore observations of their emission in the FIR, combined with optical and ultraviolet (UV) data of the light from stars, attenuated by the grains, should, in principle, strongly constrain the intrinsic distribution of stellar luminosity and dust in galaxies. This would address the fundamental question of the optical thickness of galactic disks and would allow evaluation of intrinsic quantities of interest - the star formation rate (SFR) and the star formation history. This is possible only by combining the new FIR observational results with modeling techniques for the SED from the UV to the FIR/sub-mm range. Different tools have been proposed for analyzing the energy budget of normal galaxies, starting with the pioneering works of Xu & Buat (1995) and Xu & Helou (1996) and continuing with more recent models, like those of Silva et al. (1998), Devriendt et al. (1999), Bianchi et al. (2000a). However, most of these models have made severe simplifications, which ultimately led to contradictory conclusions on the disk opacities and on the origin of the FIR emission.

Recently a new tool for the analysis of the SED in galaxies has been proposed by Popescu et al. (2000). This tool includes solving the radiative-transfer problem for a realistic distribution of absorbers and emitters, considering realistic models for dust (taking into account the grain size distribution and the stochastic heating of small grains) and the contribution of HII regions within star forming complexes. This tool was applied to the edge-on spiral galaxy NGC 891 with the result that most of the cold dust that emits in the sub-mm was embedded in a second disk of dust, associated with the young stellar population and having a very small scale height ($\sim 90 \, \text{pc}$). Subsequent application of this tool to a sample of 5 edge-on spiral galaxies (Misiriotis et al. 2001) has shown that the model seems to be generally valid and that the interpretation of the cold dust component should be ultimately analyzed in terms of SED-modeling techniques.

Another astrophysical problem related to cold dust in galaxies is the source of heating of this dust component. Here again, modeling techniques are needed for a detailed and better understanding of this component. Xu & Buat (1995) claimed that the non-ionizing UV photons constitute the main heating source of dust. However, their results were applied only to the IRAS bands, which did not reveal the bulk of the dust mass in normal galaxies, which, as we show in this paper, is in most cases too cold to have been seen by IRAS. With the advantage of the longer wavelengths observations, Popescu et al. (2000) have shown that, for the case of NGC 891, the dust emitting in the $170 - 850 \, \mu\text{m}$ regime is also predominantly heated by the UV radiation from the young stellar population. More fundamental is the accompanying result showing that the FIR colors have to be interpreted also in geometrical

terms, rather than simply as separate temperature components.

The morphology of the cold dust component and its geometrical distribution is a primary goal of the ISOPHOT Virgo project. Especially of interest is the question of whether the cold dust component extends beyond the optical disk of the galaxies, as predicted by the radiative transfer modeling analysis of the optical data of Xilouris et al. (1997, 1998, 1999) or as suggested by Alton et al. (1998a) from the analysis of the sub-mm data. Similar suggestions (Davies et al. 1999, Alton et al. 1998b) have been made on the basis of ISOPHOT maps of several nearby galaxies. However, these maps were not corrected for transient effects of the detector, and therefore both the calibration and the derived scale lengths are uncertain, and they are subject to instrumental effects.

The paper is organized as follows. Sect. 2 presents the main characteristics of our sample used for the statistical analysis of the cold dust component. The observed colors are presented in Sect. 3. In Sect. 4 dust temperatures, masses and luminosities are derived from fitting the SED of our sample galaxies. The distributions in the main derived quantities are presented in Sect. 5, and their dependence on Hubble type is investigated in Sect. 6. Sect. 7 presents the correlation of the FIR luminosity with indicators of the SFR. The implications of our analysis of the cold dust content of Virgo galaxies for our understanding of normal galaxies is discussed in Sect. 8. The summary and conclusions are given in Sect. 9.

2. Sample definition and photometric accuracy

Our sample comprises the late-type Virgo Cluster galaxies observed with the ISOPHOT instrument on board the ISO satellite. Fuller details of the selection criteria, observations, data reductions, and the catalog itself with the resulting photometry is presented in an accompanying paper (Tuffs et al. 2002). Here we give only a short description of the main aspects of the sample definition and FIR photometry relevant for the statistical investigation of cold dust in galaxies.

The observed sample consists of 63 member galaxies selected from the Virgo Cluster catalogue (VCC) (Binggeli, Sandage & Tammann 1985), with Hubble type later than S0. The galaxies were chosen to maximize the likelyhood of their belonging to the main cluster, thus minimizing the spread in distance due to the complex 3D structure (Binggeli, Popescu & Tammann 1993 and references therein). The sample is divided into cluster-core and cluster-periphery subsamples, complete to $B_{\rm T} = 14.5$ and 16.5, respectively. The 35 observed periphery galaxies are probably freshly falling in from the field (see Tully & Shaya 1984). They are principally comprised of spirals later than Sbc, irregulars and BCDs. The 28

observed core galaxies are essentially seen towards the extended X-ray halo of M 87 and are dominated by spirals of type Sc and earlier.

The observations were done using the C100 and C200 detectors, in ISOPHOT's "P32" observing mode (Tuffs & Gabriel 2001), which uses the focal plane chopper in conjunction with a spacecraft raster to rapidly sample large areas of sky. The observing wavelengths were 60, 100 and 170 μm. The "P32" mode allowed the entire optical extent of each target down to the 25.5 mag arcsec^{-2} B-band isophote and adjacent background to be scanned, while still maintaining a spatial oversampling. This allowed both spatially integrated far-IR photometry as well as information on the morphology of the galaxies in the far-IR to be extracted from the data. This paper is primarily concerned with the integrated photometry, which will include any emission from cold dust in the outer disks, where the radiation fields are weak. The most important aspect of the data reduction described by Tuffs et al. (2002) was the correction of the complex transient response behavior of the Ge:Ga photoconductor detectors of ISOPHOT. Failure to correct for this effect in data taken in the "P32" mode can give rise to serious signal losses and distortions in the derived brightness profiles through the galaxies, which in turn can lead to spurious results on the amount and distribution of cold dust in these systems. Our data are the first from the "P32" mode to have been corrected for these effects. As demonstrated by Tuffs et al. (2002) the transient-corrected photometry correlates well with IRAS observations of the brighter galaxies in our sample in the ISO 60 and 100 μm pass bands over about two orders of magnitude in integrated flux density.

From the 63 galaxies observed (61 galaxies at all three FIR wavelengths and 2 galaxies only at 100 and 170 μm) we detected 54 galaxies at least at one wavelength and 40 galaxies at all three wavelengths. From the 40 galaxies detected at all FIR wavelengths, 2 galaxies form an interacting pair (VCC 1673/1676), and their properties will be discussed in a separate paper. In this paper we largely restrict our analysis to the remaining 38 galaxies with detections at 60, 100 and 170 μm. One galaxy, VCC 1110, was observed at two additional wavelengths, 70 and 120 μm, in order to have a more detailed knowledge of the shape of the SED. This sample forms the basis for our statistical investigation. In Sect. 6, where we discuss the variation of the FIR properties with Hubble type, we add to our sample of 38 galaxies the 3 galaxies having detections only at 100 and 170 μm. The latter are introduced to increase the statistics of the BCDs (since all 3 extra galaxies are BCDs). The flux densities and their associated errors are taken from Table 7 of Tuffs et al. (2002), while the morphological types and other optical properties of the sample galaxies can be found in Table 1 of the same paper.

3. Flux density ratios

Fig. 1a shows the color-color diagram log(F170/F100) vs log(F100/F60), with the 60 and 100 μm ISO flux densities converted to the IRAS scale.[4] There is no obvious correlation, but rather a scatter diagram with the logarithm of F100/F60 ranging between $\sim$0 and 0.9 and with the logarithm of F170/F100 ranging between $\sim$0 and 0.6. Three galaxies have unusual warmer F170/F100 colors, with negative logarithmic ratios, below 0. The large scatter in the F100/F60 color can be interpreted as evidence for of a large range in star formation activity. The large scatter in the F170/F100 color indicates that cold dust is present with a large variation in dust temperatures. There is no obvious segregation with morphological type, though the galaxy with the coldest F170/F100 color is a BCD and the galaxies with the warmest F170/F100 colors are early type spirals.

Fig. 1b shows for comparison the color-color diagram of a sample of compact sources with galaxy associations detected in the ISOPHOT 170 μm serendipity survey (Stickel et al. 2000). This is the only statistical sample of galaxies observed at 170 μm existing in the literature which is also comprised of a large variety of morphological types. We will refer to this sample as to the "serendipity sample". Nevertheless the selection criteria of our sample is quite different from that of the "serendipity sample". First of all our sample is a cluster sample, while the "serendipity sample" is mainly representative of the field population. Our sample is a volume- and luminosity-limited sample, selected from an optical catalogue, while the "serendipity sample" is a blind survey at 170 μm, which will predominantly be biased towards luminous FIR sources. The redshift distribution of the latter sample (see their Fig. 4) shows that, although the majority of sources have low redshifts of $z < 0.02$, there is a long tail of redshifts up to $z \approx 0.05$. Despite the differences in the selection criteria used for the two samples, it is still useful to compare the samples and investigate their FIR properties.

The color-color diagram of the "serendipity sample' shows a slight tendency for warmer F100/F60 colors than the Virgo sample and a somewhat smaller (though still substantial) scatter in both colors. The larger scatter in our sample cannot be explained as being due to systematic calibration uncertainties, nor due to random errors (see Fig. 1a). This appears to be a real effect and one could speculate that, if there is a FIR color - FIR luminosity relation, or a relation between spread in FIR color over a population and FIR luminosity, then a sample biased towards higher FIR luminosities (as we expect the "serendipity sample"

---

[4]As shown by Tuffs et al. (2002), the flux scale of the ISOPHOT Virgo survey has a relative gain ISO/IRAS of 0.95 and 0.82 at 60 and 100 μm, respectively. These corrections have been applied to the flux densities plotted in this figure only to facilitate comparison with IRAS colors.

to be) will not reflect the full intrinsic spread in colors that a deeper sample embracing a larger proportion of low luminosity objects would. This would be consistent with more active star-forming galaxies to have narrower, warmer FIR SEDs.

4. The spectral energy distribution

The flux densities at 60, 100 and 170 μm (for a representative selection see Fig. 2[5]) indicate that for most of the galaxies of our sample the SED in the FIR peaks at wavelengths $> 100\,\mu$m and cannot be represented by a single modified black-body (Planck) function. The turn-up in the SED beyond 100 μm is a clear indication of a cold dust component which could not have been detected by IRAS. Perhaps the simplest way of quantifying this cold component would be to fit the FIR SED with 2 modified blackbody functions, one representing the so-called "warm dust" component and the other representing the so-called "cold dust" component. However, such a fit requires 4 free parameters (the amplitudes and temperatures of the "warm" and "cold" components, respectively) while there are only 3 data points available. Obviously there is an infinity of solutions which would fit the data, since the problem is mathematically under-constrained. Sub-mm data would alleviate this problem. However, long wavelength observations are not yet available for our Virgo sample. For one galaxy, VCC 1110, observations with the ISOPHOT C70 and C120 filters were made to obtain a more detailed knowledge on the shape of the SED. For this particular galaxy the fit to the data can provide a unique solution; for all the other galaxies the model fit is not unique. One way to deal with this problem is to fit a modified black-body curve only to the 100 and 170 μm data, and obtain a lower limit for the amount of cold dust and an upper limit for its temperature. Another possibility is to try to constrain the problem using some physical considerations. We use both procedures and show that they lead to the same statistical results, the differences being in the zero point of the estimated dust masses.

We first fitted the 100 and 170 μm data with one modified black-body function:

$$F_\nu \sim \nu^\beta B_\nu(T_{\rm D}) \tag{1}$$

with a fixed emissivity index $\beta = 2$. Since the ISOPHOT flux densities refer to a spectrum with $\nu F_\nu = $ constant, color corrections were first applied to the data. From the amplitude of the fitted modified black-body function dust masses were derived using the formula:

$$M_{\rm d} = \frac{4}{3}\,\frac{F_\nu\,\rho\,d^2}{Q_{\rm i}}\lambda^2\,B_\nu^{-1}(T_{\rm D}) \tag{2}$$

---

[5]The SEDs of all galaxies from our sample can be found at
$http://nedwww.ipac.caltech.edu/level5/Sept01/Popescu/Popescu\_contents.html$

where ρ is the density of the grain material ($3.2 \, \mathrm{g \, cm^{-3}}$ for silicates and $2.3 \, \mathrm{g \, cm^{-3}}$ for graphites), d is the distance to the galaxy, and Q_i is the emissivity constant ($130 \, \mu\mathrm{m}$ for silicates and $230 \, \mu\mathrm{m}$ for graphites, derived for the FIR/submm regime from Draine 1985 and consistent with the adopted emissivity index $\beta = 2$). Dust masses were calculated under the assumption of an interstellar mixture of silicates and graphites. The graphite and silicate abundances were taken from Draine & Lee (1984), namely 53% silicates (N_{Si}) and 47% graphites (N_{Graphite}) which were chosen to fit the extinction curve in our Galaxy and which we also adopted here. Dust masses and temperatures were derived for all our sample galaxies with detected 100 and $170 \, \mu\mathrm{m}$ flux densities which show evidence for two dust temperature components. In deriving dust masses and luminosities we assume that all the galaxies have the same distance, namely $11.5 \times \mathrm{h^{-1} \, Mpc}$ (see Binggeli, Popescu & Tammann 1993), where $\mathrm{h} = \mathrm{H_0}/100$ and $\mathrm{H_0}$ is the Hubble constant.

Secondly we fitted the FIR SED with two modified black-body functions by constraining one parameter of the fit. The most likely constraint is to fix the temperature of the "warm dust" component. As shown by Popescu et al. (2000) for the nearby spiral NGC 891, most of the emission at $60 \, \mu\mathrm{m}$ is due to localized FIR sources within HII regions and star forming complexes (62%). Since these results seem to be valid also for other disk galaxies (Misiriotis et al. 2001) we fixed the temperature of the "warm dust" component by making the assumption that this will represent the temperature of the average HII regions within each galaxy. Obviously this assumption neglects the fact that part of the FIR emission at $60 \, \mu\mathrm{m}$ is also due to dust heated by the diffuse optical radiation in the center of the disk (20% for NGC 891, see Popescu et al. (2000)) and by the diffuse UV radiation field in the outer parts of the disk, where small grains are stochastically heated (19% for NGC 891, see Popescu et al. (2000)). The temperature of the warm component was fixed to $47 \, \mathrm{K}$, as it provides the best fits and minimal uncertainty in the fitted parameters for all galaxies. In practice, even relatively large deviations from the $47 \, \mathrm{K}$ temperature of the warm component will not introduce large deviations in the fitted temperature of the cold component; that is, the cold dust component is quite stable against the particular shape of the warm dust component. To demonstrate this we changed the temperature of the warm component to 46

Table 1: Examples of the dependence of $T_{\mathrm{D}}^{\mathrm{cold}}$ on $T_{\mathrm{D}}^{\mathrm{warm}}$

VCC	$T_{\mathrm{D}}^{\mathrm{warm}} = 46.0 \, \mathrm{K}$	$T_{\mathrm{D}}^{\mathrm{warm}} = 47.0 \, \mathrm{K}$	$T_{\mathrm{D}}^{\mathrm{warm}} = 48.0 \, \mathrm{K}$
152	$T_{\mathrm{D}}^{\mathrm{cold}} = 18.5 \, \mathrm{K}$	$T_{\mathrm{D}}^{\mathrm{cold}} = 18.5 \, \mathrm{K}$	$T_{\mathrm{D}}^{\mathrm{cold}} = 18.4 \, \mathrm{K}$
	$\sigma = 0.5 \, \mathrm{K}$	$\sigma = 0.5 \, \mathrm{K}$	$\sigma = 0.5 \, \mathrm{K}$
318	$T_{\mathrm{D}}^{\mathrm{cold}} = 14.9 \, \mathrm{K}$	$T_{\mathrm{D}}^{\mathrm{cold}} = 14.9 \, \mathrm{K}$	$T_{\mathrm{D}}^{\mathrm{cold}} = 14.9 \, \mathrm{K}$
	$\sigma = 0.5 \, \mathrm{K}$	$\sigma = 0.5 \, \mathrm{K}$	$\sigma = 0.5 \, \mathrm{K}$

and 48 K, respectively. Table 1 shows the results for two galaxies, VCC 152 and VCC 318. The resulting fitted temperatures of the cold component and associated uncertainties are similar. Finally, the quantities derived from this procedure are compared with the fitted parameters from the one modified black-body fit.

The flux densities were again color-corrected and dust masses and temperatures were derived for all sample galaxies with detections at all three wavelengths using the same procedure outlined for one modified black-body fit. The results of the fits are listed in Table 2 and some representative examples of fitted FIR SEDs are plotted in Fig. 2. For the case of VCC 1110, where observations in more than 3 filters were available, we have used the same constrained fit and compared the predictions of the model fit with the available data at 70 and 120 μm, not used in the fit. Fig. 2 shows a very good agreement between the model predictions and the observations for this galaxy. This test is reassuring for the use of our procedure.

In order to establish whether different fitting procedures introduce internal scatter in the derived parameters of the fit we cross-correlated the dust masses obtained from fitting a single modified black-body function to the 100 and 170 μm flux densities with the dust masses of the cold component obtained from the two modified black-body fit. The correlation was tested for the galaxies with detections at all three wavelengths and which presented evidence for two dust temperature components. Fig. 3 shows a very tight correlation between the two dust masses, with only a small scatter for low dust masses (correlation coefficient 0.987). Obviously the correlation shows that using a constrained fit will give the same statistical results as the lower limits estimates, with the exception of an uncertainty in the zero point of the dust masses. Therefore for the rest of the paper we will use only the results from the constrained fit.

For 8 galaxies in our sample there was no evidence for two dust components with different temperatures, and their SED was fitted with a single modified black-body function. The parameters of these fits are listed in Table 3. These peculiar galaxies have either a very warm SED which peaks around 100 μm (VCC 836/1003/1326) or have very cold F100/F60 colors (VCC 1253/1419/1450/1725/1757) such that the 60 μm data would lie on the same modified black-body curve which is defined by the 100 and 170 μm flux densities. Most of these one temperature dust component galaxies are early-type spirals in the cluster core, some of them with Sy 2 activity (VCC836/1253) or with peculiar morphologies (VCC 1419/1757). Throughout this paper we will refer to these galaxies as to the "one component" galaxies.

5. The distributions of dust temperatures, masses and luminosities

5.1. Dust temperatures

The distribution of the cold dust temperatures ($T_{\mathrm{D}}^{\mathrm{cold}}$) is shown in Fig. 4a. The "one component" galaxies have a distinct locus in the histogram, since they form the highest temperature tail of the distribution, with values between 20 and 28 K. The most extreme example is VCC 1326 (a SBa galaxy in the cluster core) with $T_{\mathrm{D}} = 34.7$ K. For the "two component" galaxies the temperature distribution shows a wide spread in values, ranging from 12 K to 21 K. The coolest object from the distribution is VCC 655 with $T_{\mathrm{D}}^{\mathrm{cold}} = 12.6$ K. This galaxy is classified as a S pec/BCD in the cluster periphery.

The dust temperatures derived for our sample are much lower than those IRAS would have predicted on the basis of the 60 and 100 μm flux densities only. If we consider our ISO flux densities at 60 and 100 μm and only one component dust temperature we would derive a temperature distribution with a median of 26 K. This should be compared with the median value calculated for our cold dust temperature distribution, of 18.2 K - if the "one component" galaxies are included, or 16.7 K - if these galaxies are excluded. Thus the cold dust component has a median value $8 - 10$ K colder than IRAS would have predicted for our Virgo sample.

5.2. Dust masses

Most of the dust content in our sample galaxies is in form of cold dust. This can be seen from Table 2, where the tabulated cold dust masses $M_{\mathrm{D}}^{\mathrm{cold}}$ are $3 - 4$ orders of magnitude larger than the tabulated warm dust masses $M_{\mathrm{D}}^{\mathrm{warm}}$. The distribution of cold dust masses is shown in Fig. 4b. As in the temperature distribution, the "one component" galaxies have a distinct locus in the histogram, occupying the lowest mass tail of the distribution, between $4.8 < \log M_{\mathrm{D}}^{\mathrm{cold}} < 6.3\,\mathrm{M}_{\odot} \times \mathrm{h}^{-2}$. For the remaining galaxies the distribution is again very broad, extending 3 orders of magnitude in range, with a peak around $5.8\,\mathrm{M}_{\odot} \times \mathrm{h}^{-2}$. The galaxy with the largest amount of cold dust ($1.14 \times 10^{8}\,\mathrm{M}_{\odot} \times \mathrm{h}^{-2}$) is VCC 92, an Sb galaxy in the cluster periphery which is also one of the biggest galaxies in our sample, perhaps indicative of a general scaling relation between total dust mass and galaxy size.

The dust masses derived for our sample are larger than those IRAS would have predicted on the basis of the 60 and 100 μm flux densities alone. Following the same procedure as for the dust temperatures we derive an "IRAS" median value of $2.3 \times 10^{5}\,\mathrm{M}_{\odot} \times \mathrm{h}^{-2}$ and an ISO median value of $1.3 \times 10^{6}\,\mathrm{M}_{\odot} \times \mathrm{h}^{-2}$ - if the "one component" galaxies are included, or

$3.0 \times 10^6 \, \mathrm{M}_\odot \times \mathrm{h}^{-2}$ - if these galaxies are excluded. Thus our galaxy sample contains a factor $6 - 13$ more dust (for the median value) than IRAS data alone would suggest. For individual galaxies this factor could be larger.

To compensate for the effect of scaling on the dust mass distribution we have normalized dust masses in the form of dust mass surface densities, $M_\mathrm{D}^\mathrm{cold}/D^2$, where D is the major diameter[6] (in arcmin) of the galaxies measured to the faintest detectable optical surface brightness level of approximately $25.5 \, \mathrm{B} \, \mathrm{mag} \, \mathrm{arcsec}^{-2}$. The histogram of the dust mass surface densities (Fig. 4c) still shows a broad distribution, but not as broad as that in Fig. 4b. Except for the last histogram bin (one galaxy), the distribution of "two component" galaxies ranges over 2 orders of magnitudes, indicating an intrinsic variation in the amount of cold dust within galaxies. Again, the "one component" galaxies exhibit the lowest dust mass surface densities. The galaxy with the largest content of cold dust with respect to its optical size is VCC 655.

Another way of normalizing the dust masses is to take the ratio to the HI gas mass.[7] As for the case of dust mass surface densities, the distribution of dust-to-HI mass ratio $M_\mathrm{D}/M_\mathrm{HI}$ (Fig. 4d) for "two component" galaxies shows a broad distribution, ranging over two orders of magnitude. Unlike the dust mass surface densities, the distribution of dust-to-HI mass ratio for "one component" galaxies is more widely spread. The galaxy with the largest dust-to-HI mass ratio is VCC 655.

5.3. Dust luminosities

For most of our sample galaxies the FIR luminosity of the "cold component" is higher than the FIR luminosity of the "warm component" by factors of between 1.3 and 4.1 (see Table 2). For two galaxies - VCC 655 and VCC 857 - the ratio between the cold and warm FIR luminosities is as high as 6.0 and 6.1, respectively. VCC 655 is the galaxy with the coldest temperature of the cold dust component and the largest amount of dust with respect

---

[6]The diameters were taken from the VCC catalogue (Binggeli, Sandage & Tammann 1985).

[7]Most of the HI data used for normalization were taken from Bottinelli et al. (1990) and Hoffman et al. (1987). For 3 galaxies (VCC 1043/1686/1690) the average of the measurements (beam corrected) existing in the literature was considered: Bottinelli et al. (1990), Guiderdoni & Rocca-Volmerange (1985), Huchtmeier & Richter (1986) for VCC 1043; Bottinelli et al. (1990), Hoffman et al. (1987), Guiderdoni & Rocca-Volmerange (1985), Huchtmeier & Richter (1986) for VCC 1686; Bottinelli et al. (1990), Guiderdoni & Rocca-Volmerange (1985), Huchtmeier & Richter (1986), Warmels 1988 for VCC 1690. For VCC 1003, VCC 1253 and VCC 1326 the H I fluxes (beam corrected) are upper limits and come from Huchtmeier & Richter (1986).

to its optical size. VCC 857 is a SBb galaxy in the cluster periphery with LINER activity. Despite its activity the galaxy has the highest cold/warm FIR luminosity ratio. By contrast, there are two galaxies that radiate more FIR luminosity in the warm component, namely VCC 1699 (a factor 1.2) and VCC 664 (a factor 2.1). VCC 1699 is a SBm galaxy in the cluster periphery and VCC 664 is a Sc galaxy in the cluster core. One galaxy contributes equal FIR luminosity to the cold and warm component. This is the case for VCC 1554, an Sm galaxy in the cluster periphery.

The distribution of the integrated FIR luminosities for our sample galaxies (Fig. 5a) ranges over $34.0 < \log L_{FIR} < 36.4\,\mathrm{W\,h^{-2}}$. The FIR luminosities of the "cold component" (Fig. 5b) seem to be more widely distributed than the FIR luminosities of the "warm component" (Fig. 5c). This could be partly a consequence of the constraint in the fitting procedure, namely the adopted fixed temperature of the warm component. After normalization to the K′ band magnitudes[8] the distribution of the FIR luminosities (Fig. 5d) becomes slightly narrower for the "two component" galaxies. There is also a hint that the distribution of cold dust normalized luminosity (Fig. 5e) is narrower than that of the warm dust normalized luminosity (Fig. 5f). Apart from a scaling effect this might be due to a contribution of the old stellar population to the heating of cold grains.

6. FIR properties with respect to Hubble type

To study the FIR properties with respect to Hubble type we divide our sample into 4 subsamples corresponding to S0a-Sa, Sab-Sc, Scd-Sm and Im-BCDs bins in Hubble type. Ideally one would like to have very good statistics within each bin in Hubble type. Our sample has obviously the best statistics within the Sab-Sc bin and poor statistics for the Im-BCD bin. The poor statistics in the latter bin is mainly a consequence of the fact that some BCDs are only detected at two wavelengths, or only at one wavelength, and were thus not included in the overall statistics. To improve the statistics of the BCDs and to highlight their unusual properties we have added to our sample the galaxies detected only at two wavelengths (100 and 170 μm), namely VCC 130/848/1750, all of BCD class. Dust temperatures derived for these galaxies are upper limits and dust masses are lower limits (see Table 3).

The temperatures of the cold dust component (Fig. 6a) have a tendency to become

---

[8]The total K′ band magnitudes used for normalization were derived from the observations of Boselli et al. (1997) and corrected for Galactic extinction and inclination, according to the K-band corrections, as described in Gavazzi & Boselli (1996). Their median uncertainty is 0.15 mag.

colder for the later types. The early-type spirals have a temperature distribution shifted towards higher dust temperatures, with the coldest temperature only 17.7 K and the warmest 33.4 K. The broadest temperature distribution is exhibited by the Sab-Sc spirals, with $14 < T_{\mathrm{D}}^{\mathrm{cold}} < 28$ K. The later spirals and irregulars have a distribution shifted towards colder dust temperatures, with the BCDs having the coldest dust temperatures. The BCD VCC 655 has the coldest dust temperature (12.6 K) among the galaxies with 3 wavelengths detection. Of the BCDs detected only at two wavelengths, VCC 848 has the coldest dust temperature, 9.9 K as an upper limit. The median values of the dust temperatures (Table 4) are in agreement with the early-type spirals having the warmest median temperature and the BCDs having the coldest median temperature.

Table 4: Median values for the temperatures and mass surface densities within each bin of Hubble type

type	T_{median}	$(M/D^2)_{\mathrm{median}}$
	K	$\mathrm{M}_\odot \times \mathrm{h}^{-2} \times \mathrm{arcmin}^{-2}$
S0a-Sa	20.5	3.4×10^4
Sab-Sc	16.1	3.2×10^5
Sd-Sm	18.5	2.1×10^5
Im-BCD	15.9	1.2×10^6

The distribution of cold dust masses (Fig. 6b) shows a pronounced effect of the scaling relations, with the Sab-Sc spirals having the largest amount of dust, as expected for more massive galaxies. However, in the dust mass surface density distributions (Fig. 6c) there is a trend for the early spirals to have small dust masses per unit area and for the BCDs to have the larger amounts of dust compared to their optical sizes. The BCDs VCC 655 and VCC 848 are the most extreme examples. The median of the dust mass surface density (Table 4) has the lowest value for the early-type spirals and the largest value for the BCDs. There is no obvious trend in the distributions of the dust-to-HI mass ratio (Fig. 6d) with respect to Hubble type.

The distributions of FIR luminosities (Fig. 7a) are mainly dominated by the scaling effects, with the more massive galaxies (Sbc-Sc) having the larger FIR luminosities. Only after normalization to the K′-band magnitudes (Fig. 7d) does it become obvious that there is a trend for the early-type spirals to have intrinsically low total FIR luminosities; this is mainly attributable to the "one component" galaxies.

Within the available statistics there was no evidence for a strong segregation between cluster periphery and cluster core galaxies within morphological classes. The only exception might be the tendency for cluster core early type spirals (which are known to have the most

extreme HI deficiencies) to be lacking cold dust components.

7. Correlations with indicators of SFR

7.1. The FIR-Hα correlation

The Hα equivalent widths (EW) measure the strength of the mass-normalized recent
($< 10^8$ yr) SFR. To study the correlation between the Hα EW and the FIR emission for
our sample galaxies we made use of the data available in the literature, namely Hα+[NII]
EW obtained from long-slit (from 3 to 7 arcmin) spectroscopy (Kennicutt & Kent 1983)
or from CCD imaging (Gavazzi, private communication). Their typical uncertainty is $2\,\mathring{A}$.
Fig. 8a and 8b show the normalized FIR luminosities of the warm and cold dust components,
respectively, versus the Hα (+[NII]) equivalent widths (EW). The linear correlation found for
the warm component is consistent with, and a necessary condition for our original premise
for the constrained fit, namely the identification of the warm component with localized HII
regions.

To better understand the trends in the correlations we consider below the bolometric
energy budget as a function of the recent SFR, in the case of a 3 component model consisting
of: locally heated dust in star-forming complexes, diffuse dust heated by the non-ionizing
UV photons, and diffuse dust heated by the optical photons. Such a model does not take
into account the existence of cold dust associated with clumps (quiescent or associated with
molecular clouds), which may need a separate treatment. However, if the cold dust is only
in a diffuse component, the relation between SFR and the total FIR energy output can be
derived from the following equation:

$$L_{\mathrm{FIR}}^{\mathrm{tot}} = L_{\mathrm{FIR}}^{\mathrm{HII}} + L_{\mathrm{FIR}}^{\mathrm{UV}} + L_{\mathrm{FIR}}^{\mathrm{opt}} \tag{3}$$

where $L_{\mathrm{FIR}}^{\mathrm{tot}}$ is the total FIR luminosity emitted by the galaxy, $L_{\mathrm{FIR}}^{\mathrm{HII}}$ is the FIR luminosity
emitted by the HII regions and star forming complexes, $L_{\mathrm{FIR}}^{\mathrm{UV}}$ is the FIR luminosity of the
diffuse dust component heated by the non-ionizing UV photons and $L_{\mathrm{FIR}}^{\mathrm{opt}}$ is the FIR lumi-
nosity of the diffuse dust component heated by the optical photons. The equation can be
further expressed in terms of SFR:

$$L_{\mathrm{FIR}}^{\mathrm{tot}} = SFR \times (L_0 \times F + L_x \times X) + SFR \times L_0 \times (1 - F) \times G_{uv} + L_{\mathrm{FIR}}^{\mathrm{opt}} \tag{4}$$

where SFR is the present-day star formation rate in $M_\odot$/yr, L_0 and L_x are the non-ionizing
and the ionizing UV bolometric luminosities of a young stellar population corresponding to
$SFR = 1\,M_\odot$/yr (which can be derived from population synthesis models), F and X are the

fractions of non-ionizing and ionizing UV emission that is absorbed by dust locally within star forming complexes, and the factor G_{uv} is the probability that a non-ionizing UV photon escaping from the star formation complexes will be absorbed by dust in the diffuse interstellar medium. The ionizing UV is thought by most authors to be mainly locally absorbed by gas in the HII regions. Its contribution to $L_{\mathrm{FIR}}^{\mathrm{HII}}$ is in any case small, and its effect on the heating of dust in the diffuse ISM can be totally neglected.

The warm dust component from our fitting procedure was identified with the dust locally heated within the HII regions, such that $L_{\mathrm{FIR}}^{\mathrm{warm}} \simeq L_{\mathrm{FIR}}^{\mathrm{HII}}$. In this case we indeed expect a linear correlation with the SFR and thus with the EW,

$$L_{\mathrm{FIR}}^{\mathrm{warm}} \simeq SFR \times (L_0 \times F + L_x \times X) \tag{5}$$

The scatter in the correlation of Fig. 8a is only to be expected due to the possible contribution of the diffuse component to the $60\,\mu$m band via stochastic emission, heating by the old stellar population (see Popescu et al. 2000), and the likely variation in HII region dust temperatures within and between galaxies (e.g. due to the effect of metallicity on the hardness of the stellar photons and/or due to effects of star-burst age). To this we should add the uncertainty of ~ 0.3 dex in the value of the Hα EW (due to measurement errors in determining the continuum emission as well as to the [NII] contamination), which can also contribute to the scatter.

If the cold dust component is identified with diffuse dust heated by the interstellar radiation field, then:

$$L_{\mathrm{FIR}}^{\mathrm{cold}} \simeq SFR \times L_0 \times (1 - F) \times G_{uv} + L_{\mathrm{FIR}}^{\mathrm{opt}} \tag{6}$$

Fig. 8b suggests that there is also a correlation, though non-linear, and with a larger scatter, for the cold component. The correlation coefficient is 0.75 if we consider all the data points or 0.83 if we exclude the extreme point above the correlation (at log EW(Hα)=0.7). The excluded galaxy is a BCD, and we have already mentioned the unusual properties of these galaxies. The correlation itself suggests that the cold dust component is predominantly heated by the non-ionizing UV radiation produced by the young stellar population, consistent with the model predictions of Popescu et al. (2000) and Misiriotis et al. (2001). To explain the non-linearity in the correlation based on the model described above we can invoke either a variation of the G_{uv} factor with Hα EW or a strong influence of $L_{\mathrm{FIR}}^{\mathrm{opt}}$ for small Hα EW. The F factor is taken to be invariant within our sample, an assumption validated by the linear correlation obtained in Fig. 8a. The first possibility would imply that more active galaxies have lower G_{uv} factors (less optically thick disks). This seems unlikely, as starburst galaxies are known to be more optically thick systems compared to normal galaxies. The second

possibility simply states that more quiescent galaxies should have a higher contribution from the optical photons in heating the dust. Scatter in the correlation is again to be expected due to the varying contribution of the old stellar population in heating the dust and to some varying degree of clumpiness of the interstellar medium within galaxies.

7.2. The FIR-radio correlation

Another important correlation with indicators of SFR is the well known FIR-radio correlation. Discovered during the IRAS mission, the FIR-radio correlation was probed not only in terms of absolute fluxes (e.g. Helou, Soifer & Rowan-Robinson 1985, de Jong et al. 1985, Wunderlich, Wielebinski & Klein 1987) but also in flux per unit galactic mass (Xu et al. 1994). Basically the correlation holds for the integrated emission. The link is qualitatively given by the grain heating associated with the appearance of massive stars and the acceleration of relativistic particles in their eventual SN explosions. However, the tightness of the correlation appears to constrain the characteristics of late-type galaxies to rather more specific properties: an optical thickness of the disk that is of order unity for non-ionizing stellar UV radiation (Xu 1990), a magnetic field energy density that is about equal to that of the radiation field over more than an order of magnitude in dynamic range, and radiative energy losses of the synchrotron electrons that exceed escape losses, so that the galaxies act for both energy inputs as calorimeters (Völk 1989, Lisenfeld, Völk & Xu 1996).

Previous studies of the FIR-radio correlation were confined to the IRAS fluxes, and to FIR luminosites obtained by extrapolating the IRAS fluxes. Our new ISOPHOT data, and in particular our finding of a cold dust component present within all morphological classes naturally raises the question of whether the FIR luminosity associated with the cold component is also correlated with the radio emission. Popescu et al. (2000) have shown that in NGC 891 there is a relative increase of the contribution of the UV photons to the heating of the diffuse interstellar dust with increasing FIR wavelengths, such that in the sub-mm regime the dust emission is mainly powered by the UV photons ($\sim 60\%$). If this is the case one would also predict a tight correlation for the FIR emission of the cold dust component with the radio emission, since the stars mainly responsible for the heating of the cold dust also give rise to most of the radio emission. Fig. 9a, b show a good correlation between the FIR luminosities of both the warm and cold dust components, and the NVSS (NRAO VLA Sky Survey) radio luminosites at 1.4 GHz taken from Gavazzi & Boselli (1999). The interpretation of the correlations is limited by the poor statistics, since only 14 galaxies from our sample have NVSS detections. Nevertheless, some interesting features are apparent.

First of all, the prediction regarding the validity of the FIR-radio correlation for the cold dust component is confirmed. Secondly, there is a clear non-linearity in both correlations.

The non-linear warm FIR-radio correlation plotted in Fig. 9a (FIR/radio < 1 and with a correlation coefficient 0.85), is similar (within the poor statistics) to that obtained by Xu, Lisenfeld & Völk (1994). However, the "warm" and "cold" FIR components from Xu et al., as derived from the IRAS observations, are not to be identified with our "warm" and "cold" dust components, despite a common physical justification. The non-linearity of the correlation is an interesting effect, which at present is difficult to explain. Because of the weak dependence of the radio synchrotron intensity on the B field predicted by the original calorimeter theory, consistent with observed radio spectral indices (Lisenfeld & Völk 2000), the non-linearity in the warm FIR-radio correlation should be small. The scatter in the warm FIR-radio correlation has probably several components: the intrinsic scatter of the FIR-radio correlation (see Xu, Lisenfeld & Völk 1994), and, as for the case of the warm-FIR Hα correlation, components due to effects of stochastic heating of dust in low density radiation fields and to optical heating of dust in high density radiation fields, in optically thick regions in the very central part of galaxies.

The non-linear cold FIR-radio correlation plotted in Fig. 9b (FIR/radio < 1 but closer to slope unity and with a correlation coefficient 0.85) is again similar to that obtained by Xu, Lisenfeld & Völk (1994). Unlike the case of the warm FIR-radio correlation, the non-linearity of the cold FIR-radio correlation can be explained by invoking a higher relative contribution to the heating of diffuse dust by the old stellar population in galaxies with lower present day SFR (Xu et al. 1994). The scatter of the correlation has again to be viewed in terms of several components, where one component is attributable to the contribution of varying proportions of optical photons in heating the dust.

8. Discussion

The statistical analysis of the integrated FIR properties of our Virgo sample unambiguously shows the existence of a cold dust component present in all morphological classes of late-type galaxies, from early spirals to irregulars and BCDs. Here we consider the implications of this analysis for the nature of the cold dust component.

A basic question arising from our analysis concerns the location and morphology of the cold dust component. One argument in favor of a diffuse origin for this component is the lack of a cold component in some Virgo cluster core early type galaxies with HI deficiencies. Though statistics are poor, this may point towards a diffuse dust component which is absent

because of stripping. Another hint for a diffuse origin of the cold component is the non-linear correlation between the normalized luminosity of the cold dust component and the Hα EW seen in Fig. 8b, which was interpreted in terms of a diffuse dust component heated by both UV and optical photons, with the main contribution coming from the UV radiation (as predicted by Popescu et al. 2000, Misiriotis et al. 2001). Finally, the cold FIR-radio correlation is again consistent with the predictions of the Popescu et al. (2000) model, where the bulk of the cold FIR emission arises from diffuse dust heated by UV photons.

A fundamental issue is the amount of dust in galaxies. We find large amounts of dust in galaxies, significantly higher than derived from IRAS data alone. The missing dust, not seen by IRAS, is present within all morphological types of galaxies, from early spirals to irregulars and BCDs. However, what we can really measure is dust opacity to starlight, and what we derive as dust mass depends on several assumptions. It is not only the fact that SED fits are ambiguous with respect to a zero point (see Sect. 4), but also the possibility that some dust might be located in compact optically thick sources. In such cases dust may have different optical properties, and in particular ices may be present. These have stronger mass-normalized absorption coefficients in the FIR-submm regime (e.g. Preibisch et. al. 1993), which would reduce the implied dust-to-gas ratios for these regions.

Perhaps the most intriguing result of this investigation are the masses and temperatures of the cold dust derived for the BCD galaxies in our sample. These systems are clearly differentiated from the spirals, having the highest dust mass surface densities (normalized to optical size), and the lowest dust temperatures (ranging down to less than $10\,\mathrm{K}$). This is not the expected behavior for galaxies whose FIR emission is dominated by dust heated locally in HII regions, where one would anticipate temperatures of $30\,\mathrm{K}$ or more. This was the a priori expectation in particular for the BCDs, and was the standard interpretation for the IRAS results obtained for these systems (see for example Hoffman et al. 1989, Helou et al. 1988, Melisse & Israel 1994, who found that the $60/100\,\mu$m colors of BCDs - including examples from the Virgo cluster - were clearly warmer than for spirals). Our findings indicate a cold dust component supplementary to the warm dust component detected by IRAS. This in itself is not surprising, as it is to be expected that cold dust associated with the star formation regions (SFRs) should be present at some level in association with the molecular component detected in CO. The particularly unexpected aspect of this is rather that the luminosity of the cold dust component should dominate over that of the warm dust, as shown by the failure to detect systems (which are clearly seen at 170 micron), in one or both of the ISOPHOT 60 and $100\,\mu$m bands.[9] An equally strong observational constraint is given

---

[9]The integrated Blue magnitudes of the BCDs in our sample are fainter than the BCDs detected by IRAS by typically two magnitudes.

by the ratio of observed luminosity of the cold dust component compared with the observed (i.e. not corrected for intrinsic absorption) luminosity in B-band.[10] This ranges from 6 to 60 percent over the sample of BCDs.

Here we qualitatively discuss the nature of the cold dust emission detected by ISO in Virgo Im and BCD galaxies, considering in general terms the origin and location of the grains, and their heating. For photon-heated dust, low grain temperatures might be reached in dense clouds opaque to the ambient radiation fields in the galaxies, provided the clouds were quiescent (i.e. not harboring star forming regions which would give rise to a warm FIR emission component dominating the bolometric output of the clouds.) However, clouds with filling factors of perhaps a few percent would only be expected to intercept and reradiate a corresponding few percent of the UV-optical output of the galaxy. By contrast, perhaps a few tens of percent of the UV-optical output of these systems appears in the cold dust component.

Alternatively, the grains could be distributed in a diffuse component sufficiently extended that the interstellar radiation field (ISRF) would be weak enough to lead to grain temperatures of order $10\,$K or less. Such grains would have to be distributed over dimensions of order $10\,$kpc around the central star-forming area in the BCDs (of extent typically of order a kpc). The grains would be embedded in the surrounding intergalactic medium (IGM), most probably in the putative protogalactic cloud from which the galaxy formed. Such an explanation might explain the extreme cold dust surface densities for Im and BCD galaxies, which would be reduced to values more compatible with spirals if the surface area normalization were to be with respect to a radius compatible with the cold dust temperature rather than with respect to the B-band extent of the galaxies. Furthermore, there is evidence that the 170μm emission is resolved in two BCDs, VCC 1 and VCC 848 (see Fig. 5 of Tuffs et al. 2002). However, if such grains are photon-heated, significant optical depths in the diffuse component would be required to convert substantial fractions of the UV-optical output into FIR photons, as observed in some objects. In their sample of 13 field BCDs, Hunter & Hoffman (1999) found E(B-V) to be distributed in the range $0.00 - 0.53$, with evidence for optical colors being affected by a diffuse dust component.

Another possibility to account for FIR emission of the observed luminosity, color and extent would be to invoke collisional, rather than radiative heating for the extended cold dust emission component. In particular, BCD galaxies are thought to undergo sporadic episodes of star formation activity (Mas-Hesse & Kunth 1999), giving rise to a galactic wind

---

[10]This was estimated by taking the B_T magnitudes from Binggeli, Sandage and Tammann (1985) and converting to fluxes using conversion factors tabulated in Matthews & Sandage (1963).

which interacts with the protogalactic cloud. This creates a wind bubble containing shocked coronal swept-up gas, in which any embedded grains will be collisionally heated. If collisional grain heating were to constitute the dominant cooling mechanism for the shocked swept up IGM, the observed FIR luminosity and color of the cold dust emission from the Virgo BCD galaxies could be explained.

A detailed description of the circumstances under which such an efficient conversion of mechanical wind luminosity into FIR radiation occurs, is beyond the scope of this paper. The general analytical solutions of Weaver et al. (1977) can be applied to the gas density and temperature profiles of a spherical wind bubble, to explore the conditions under which we may expect the internal energy of the coronal gas in the shocked swept up IGM region to be converted predominantly into FIR radiation, as required by the observations. In essence, this can only occur if sufficient dust is present in the shocked IGM that the timescale for gas cooling through inelastic collisions with grains is both shorter than the timescale for cooling through line emission, as well as being less than or comparable to the dynamical timescale. This scenario would have interesting implications for the interpretation of the integrated FIR emission of dwarf star-forming galaxies in the distant universe, implying that some fraction of the FIR luminosity had a mechanical, rather than photon-powered origin. One immediate observational consequence would be a larger color ratio $L_{\mathrm{FIR}}/L_{\mathrm{UV-opt}}$ for the ensemble of cosmologically distant dwarf star-forming systems than would be expected on the basis on photon heating alone, as we have directly observed for our sample of Virgo BCD systems.

A rather different scenario explaining the high dust mass and dust surface densities would come back to a spatially extended grain population that is asymmetrically distributed around the optical-UV emitting central star-forming region. This could be a (flaring) disk of accreting material that feeds the star forming center. BCDs would then be those members of such asymmetric systems seen under favorable aspect angle for observation of the central optical-UV emission. Systems seen edge-on would be FIR-dominated by photon heating and possibly not yet detected as a group in the visual range. They would only show up in the FIR and sub-mm range, where the only major blind search up to now is the ISOPHOT $170\,\mu\mathrm{m}$ serendipity survey. It will be interesting to search for such objects in the serendipity sample. In the extreme case BCDs - or a significant sub-class of them - would be dwarf galaxies that undergo a massive gas/dust accreting phase that makes them (at least sporadically) bright optical-UV sources. Collisional dust heating might occur in addition as a consequence of dynamical effects like wind interactions in the broader environment, as described above.

9. Summary

Based on observations taken in the P32 mode of the ISOPHOT instrument on board ISO we have statistically analyzed the integrated FIR properties of a complete volume- and luminosity-limited sample of late-type Virgo Cluster galaxies. For the first time, data taken in this observing mode could be corrected for the complex non-linear response of the detectors, allowing robust integrated photometry to be extracted, and over the entire optical extent of the galaxies, including the outer regions of the galactic disks. We demonstrate the existence of a cold dust component present within all the morphological classes observed, which range from S0a to Im and BCD. This cold component, which was not previously seen by IRAS, was analyzed by fitting the data with a superposition of two modified black-body functions of form $\nu^2 B_\nu$, physically identified with a localized warm dust emission component associated with HII regions (whose temperature was constrained to be $47\,\mathrm{K}$), and a diffuse emission component of cold dust. The fits imply a revision of the masses and temperatures of dust in galaxies.

The main results are summarized as follows:

- The dust masses should be raised by factors of $6 - 13$ from the previous IRAS determinations, with even larger factors for certain individual galaxies. The temperature of the cold dust is found to be generally $8 - 10\,\mathrm{K}$ lower than the IRAS temperatures, again with individual galaxies having even lower temperatures.

- The temperatures of the cold dust component have a tendency to become colder for the later types. The early-type spirals have a distribution in cold dust temperatures shifted towards higher values, with the coldest and warmest temperatures of $17.7\,\mathrm{K}$ and $33.4\,\mathrm{K}$. The later spirals and irregulars have a distribution shifted towards lower dust temperatures, with the BCDs having the coldest dust temperatures (ranging down to less than $10\,\mathrm{K}$).

- There is a trend for the early spirals to have small dust masses per unit area and for the BCDs to have the largest amounts of dust normalized to their optical sizes.

- The BCD galaxies were found to have the highest dust mass surface densities (normalized to optical area) and the coldest dust temperatures of the galaxies in the sample. This is a particularly unexpected result, since the IRAS observations of BCDs could be accounted for in terms of dust heated locally in HII regions, with temperatures of $30\,\mathrm{K}$ or more. Two scenarios invoking collisionally or photon-heated emission from grains originating in the surrounding intergalactic medium are proposed to qualitatively account for the FIR and optical extinction characteristics of BCDs. In the one scenario,

grains are swept up from a surrounding protogalactic cloud and heated collisionally in an optically thin wind bubble blown from the BCD. In the other, the grains are taken to be photon-heated in an optically thick disk surrounding the optical galaxy. The disk is indicative of a massive gas/dust accreting phase which makes dwarf galaxies sporadically bright optical-UV sources when viewed out of the equatorial plane of the disk. Elements of both scenarios may apply to real-life BCDs.

- A good linear correlation is found between the "warm FIR" luminosities and the Hα EW. This is in agreement with the assumptions of our constraint SED fit, that the "warm" component is mainly associated with dust locally heated within star forming complexes. We also found a good but non-linear correlation between the "cold FIR" luminosities and the Hα EW. The correlation itself confirms the predictions of the Popescu et al. (2000) model, where the emission at FIR-sub-mm wavelengths is mainly due to the diffuse UV photons.

- A non-linear correlation is found between the "warm" FIR luminosities and the NVSS radio luminosities at $1.4\,$GHz. A good FIR-radio correlation was also found for the cold dust component, suggesting that the stars mainly responsible for heating the cold dust are the massive progenitors of supernovae whose remnants may be the dominant sources of cosmic ray electrons. Our findings are the first ones to test the FIR-radio correlation using the FIR luminosities associated with the cold dust component.

REFERENCES

Alton, P. B., Bianchi, S., Rand, R. J., Xilouris, E. M., Davies, J. I., & Trewhella, M. 1998a, ApJ, 507, L125

Alton, P. B., Trewhella, M., Davies, J. I., Evans, R., Bianchi, S., Gear, W., Thronson, H., Valentijn, E., & Witt, A. 1998b, A&A, 335, 807

Alton, P. B., Lequeux, J., Bianchi, S., Churches, D., Davies, J., & Combes, F. 2001, A&A, 366, 451

Bianchi, S., Davies, J I., & Alton, P.B. 2000a, A&A, 359, 65

Bianchi, S., Davies, J. I., Alton, P. B., Gerin, M., & Casoli, F. 2000b, A&A, 353, L13

Binggeli, B., Popescu, C. C. & Tammann, G. A. 1993, A&AS, 98, 275

Binggeli, B., Sandage, A. & Tammann, G. A. 1985, AJ, 90, 1681

Boselli, A., Tuffs, R. J., Gavazzi, G., Hippelein, H., & Pierini, D., 1997, A&AS, 121, 507

Bottinelli, L., Gouguenheim, L., Fouquè, P., & Paturel, G. 1990, A&AS, 82, 391

Braine, J., Krügel, E., Sievers, A., & Wielebinski, R. 1995, A&A, 295, L55

Braine, J., Guélin, M., Dumke, M., Brouillet, N., Herpin, F., & Wielebinski, R. 1997, A&A, 326, 963

Chini, R., Kreysa, E., Krügel, E., & Mezger, P. G. 1986, A&A, 166, L8

Contursi, A., Boselli, A., Gavazzi, G., Bertagna, E., Tuffs, R., & Lequeux, J. 2001, A&A, 365, 11

de Jong, T., Klein, U., Wielebinski, R., & Wunderlich, E. 1985, A&A, 147, L6

Davies, J. I., Alton, P., Trewhella, M., Evans, R., & Bianchi, S. 1999, MNRAS, 304, 495

Devereux, N. A., & Young, J. 1993, AJ, 106, 948

Devriendt J. E. G., Guiderdoni B., & Sadat R. 1999, A&A, 350, 381

Draine, B. T. 1985, ApJS, 57, 587

Draine, B. T., & Lee, H. M. 1984, ApJ, 285, 89

Dumke, M., Braine, J., Krause, M., Zylka, R., Wielebinski, R., & Guélin, M. 1997, A&A, 325, 124

Engargiola, G. 1991, ApJS, 76, 875

Gavazzi, G., & Boselli, A., 1996, in: A UBVJHK photometric catalogue of 1022 galaxies in 8 nearby clusters, Gordon and Breach Science Publishers, New York

Gavazzi, G., & Boselli, A. 1999, A&A, 343, 86

Guélin, M., Zylka, R., Mezger, P. G., Haslam, C. G. T., & Kreysa, E. 1995, A&A, 298, L29

Guélin, M., Zylka, R., Mezger, P. G., Haslam, C. G. T., Kreysa, E., Lemke, R., & Sievers, A. W. 1993, A&A, 279, L37

Lisenfeld, U. & Völk, H. J., 2000, A&A, 354, 423

Guiderdoni, B, & Rocca-Volmerange, B. 1985, A&A, 151, 108

Haas, M., Lemke, D., Stickel, M., Hippelein, H., Kunkel, M., Herbstmeier, U., & Mattila, K. 1998, A&A, 338, L33

Helou, G., Soifer, B. T., & Rowan-Robinson, M. 1985, ApJ, 298, L7

Helou, G., Khan, I. R., Malek, L., & Boehmer, L. 1988, ApJS, 68, 151

Hoffman, G. L., Helou, G., Salpeter, E. E., Glosson, J., & Sandage, A. 1987, ApJS, 63, 247

Hoffman, G. L., Helou, G., Salpeter, E. E., & Lewis, B. M. 1989, ApJ, 339, 812

Huchtmeier, W. K., & Richter, O. G. 1986, A&AS, 64, 111

Hunter, D. A. & Hoffman, L. 1999, AJ, 117, 2789

Israel, F. P., Van Der Werf, P. P., & Tilanus, R. P. J. 1999, A&A, 344, L83

Kennicutt, R. C., & Kent, S. M. 1983, AJ, 88, 1094

Kessler, M. F., Steinz, J. A., Anderegg, M. E., Clavel, J., Drechsel, G., Estaria, P., Fälker, J., Riedinger, J. R., Robson, A., Taylor, B. G., & Ximenéz de Ferrán, S. 1996, A&A, 315, 27

Krügel, E., Siebenmorgen, R., Zota, V., & Chini, R. 1998, A&A, 331, L9

Lemke, D., Klaas, U., Abolins, J., Ábráham, P., Acosta-Pulido, J., Bogun, S., Castañeda, H., Cornwall, L., Drury, L., Gabriel, C., Garzón, F., Gemünd, H. P., Grözinger, U., Grün, E., Haas, M., Hajduk, C., Hall, G., Heinrichsen, I., Herbstmeier, U., Hirth, G., Joseph, R., Kinkel, U., Kirches, S., Kömpe, C., Krätschmer, W., Kreysa, E., Krüger, H., Kunkel, M., Laureijs, R., Lützow-Wentzky, P., Mattila, K., Müller, T., Pacher, T., Pelz, G., Popow, E., Rasmussen, I., Rodríguez Espinosa, J., Richards, P., Russell, S., Schnopper, H., Schubert, J., Schulz, B., Telesco, C., Tilgner, C., Tuffs, R. J., Völk, H. J., Walker, H., Wells, M., & Wolf, J. 1996, A&A, 315, L64

Lisenfeld, U., Völk, H. J., & Xu, C. 1996, A&A, 306, 677

Mas-Hesse, J. M. & Kunth, D. 1999, A&A, 349, 765

Matthews, T. A. & Sandage, A. R. ApJ, 138, 30

Melisse, J. P. M., & Israel, F. P. 1994, A&A, 285, 51

Misiriotis A., Popescu, C. C., Tuffs, R. J., & Kylafis, N. D. 2000, A&A, 372, 775

Neininger, N., Guélin, M., García-Burillo, S., Zylka, R., & Wielebinski, R. 1996, A&A, 310, 725

Popescu, C. C., Misiriotis A., Kylafis, N. D., Tuffs, R. J., & Fischera, J., 2000, A&A, 362, 138

Preibisch, Th., Ossenkopf, V., Yorke, H. W. & Henning, Th. 1993, A&A, 279, 577

Siebenmorgen, R., Krügel, E., & Chini, R. 1999, A&A, 351, 495

Sievers, A. W., Reuter, H. -P., Haslam, C. G. T., Kreysa, E., & Lemke, R. 1994, A&A, 281, 691

Silva L., Granato G.L., Bressan A., & Danese L. 1998, ApJ, 509, 103

Stickel, M., Lemke, D., Klaas, U., Beichman, C. A., Rowan-Robinson, M., Efstathiou, A., Bogun, S., Kessler, M. F., & Richter, G. 2000, A&A, 359, 865

Trewhella, M., Davies, J. I., Alton, P. B., Bianchi, S., & Madore, B. F. 2000, ApJ, 543, 153

Tuffs, R. J. & Gabriel, C. 2002, A&A, in preparation

Tuffs, R. J., Popescu, C. C., Pierini, D., Völk, H. J., Hippelein, H., Leech, K., Metcalfe, L., Heinrichsen, I., & Xu, C. 2002, ApJS in press

Tuffs, R. J., Lemke, D., Xu, C., Davies, J. I., Gabriel, C., Heinrichsen, I., Helou, G., Hippelein, H., Lu, N. Y., & Skaley, D. 1996, A&A, 315, L149

Tully, R. B. & Shaya, E. J. 1984, ApJ, 281, 31

Völk, H. J. 1989, A&A, 218, 67

Warmels, R. H. 1988, A&AS, 72, 427.

Weaver, R., McCray, R., Castor, J., Shapiro, P., & Moore, R. 1977, ApJ, 218, 377

Wunderlich, E., Wielebinski, R., & Klein, U. 1987, A&AS, 69, 487

Xilouris E. M., Kylafis N. D., Papamastorakis J., Paleologou E. V., & Haerendel G. 1997, A&A, 325, 135

Xilouris E. M., Alton P. B., Davies J. I., Kylafis, N., Papamastorakis, J., & Trewhella, M. 1998, A&A, 331, 894

Xilouris E. M., Byun Y. I., Kylafis N. D., Paleologou E. V., & Papamastorakis J. 1999, A&A, 344, 868

Xu, C. 1990, ApJ, 365, L47

Xu C., & Buat V. 1995, A&A, 293, L65

Xu C., & Helou G. 1996, ApJ, 456, 163

Xu C., Lisenfeld U., & Völk H. J. 1994, A&A, 285, 19

Xu, C., Lisenfeld, U., Völk, H. J., & Wunderlich, E. 1994, A&A, 282, 19

(a)   (b)
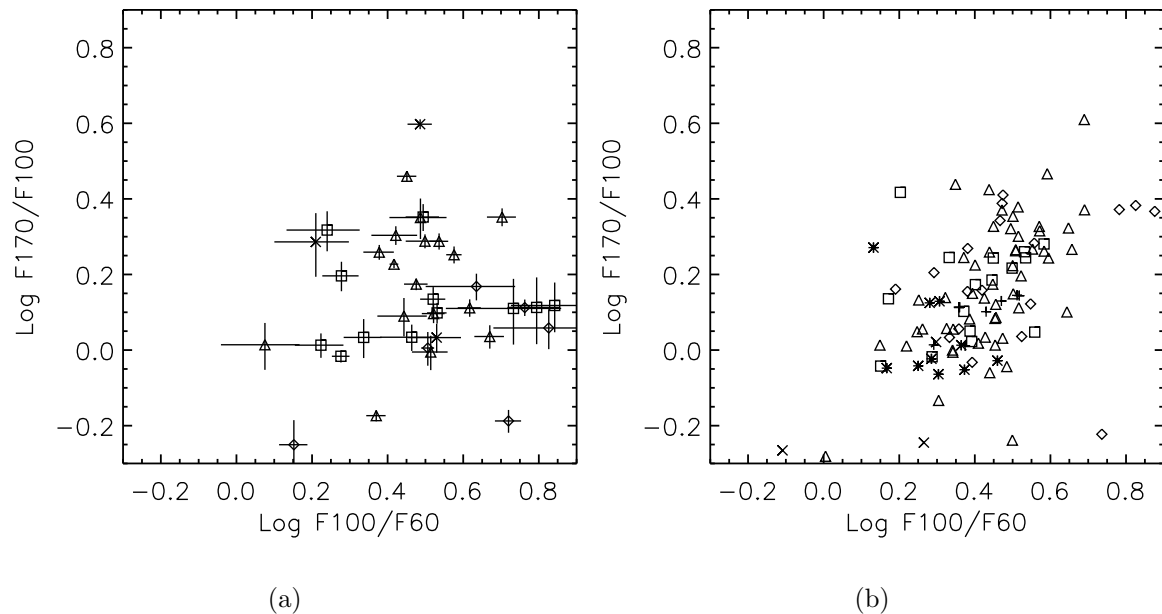
Fig. 1.— a) The color-color plot of our sample galaxies with detections at all three wave-
lengths. The 60 and $100\,\mu$m flux densities have been converted to the IRAS flux scale.
Random uncertainties in the color ratios are plotted as bars (half length $1\,\sigma$). b) The color-
color plot from the "serendipity sample" (Stickel et al. 2000). Different Hubble types are
plotted as follows: diamonds: S0-Sa, triangles: Sb-Sc, squares: Sd-Sm, crosses: Im-BCD,
plus-signs: S galaxies, stars: unclassified. The last two symbols refer to the "serendipity
sample".
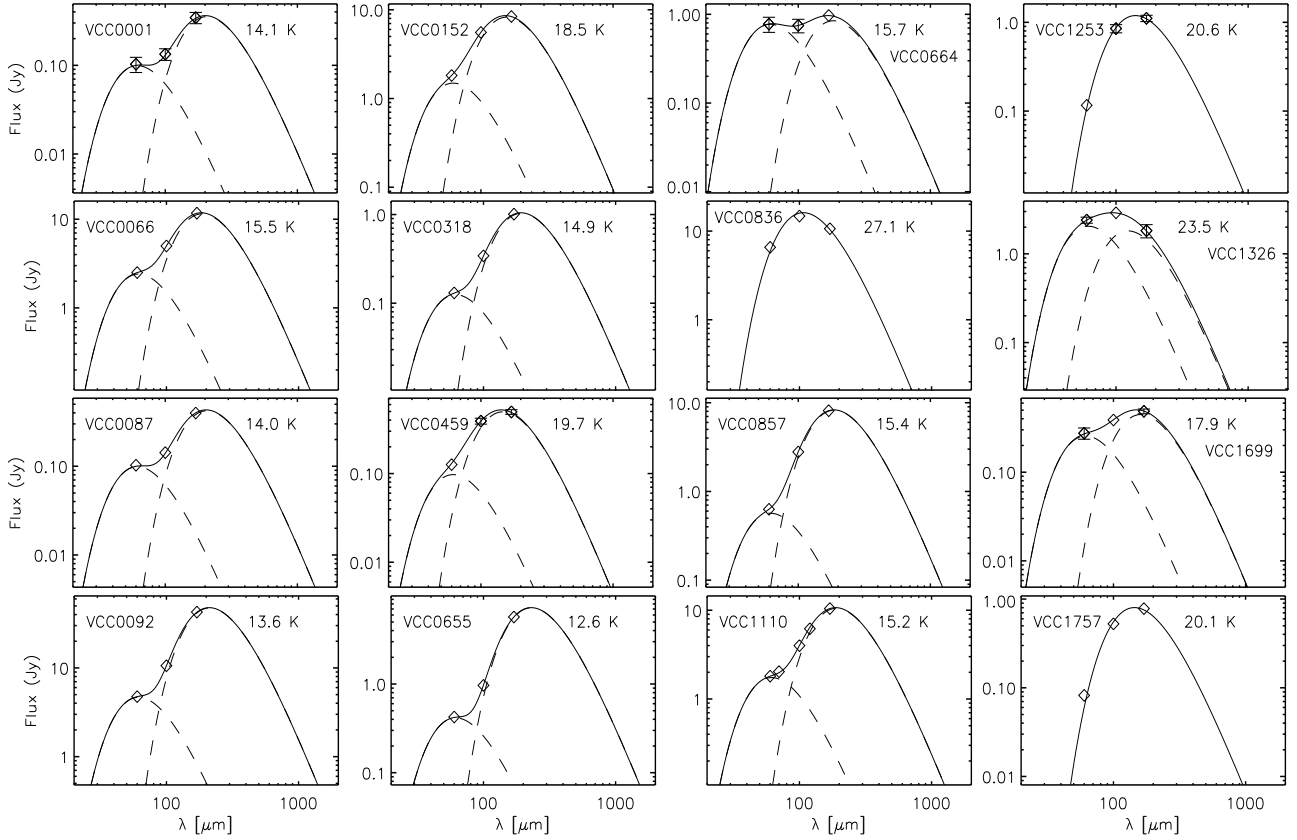
Fig. 2.— Examples of FIR SEDs from our sample galaxies. The color corrected flux densities at 60, 100 and 170 μm are plotted together with their associated error bars. One galaxy, VCC 1110 has additional measurements at 70 and 120 μm. The two modified black-body functions which best fitted the data points are plotted with dashed-lines. The temperature of the warm component is constrained to be 47 K. The fitted temperature of the cold component is marked near each fit. The sum of the two fitting functions is plotted as the solid line. Some galaxies (see text) don't show evidence for two dust components and their SEDs are fitted with single component modified black-body functions, plotted as solid lines.
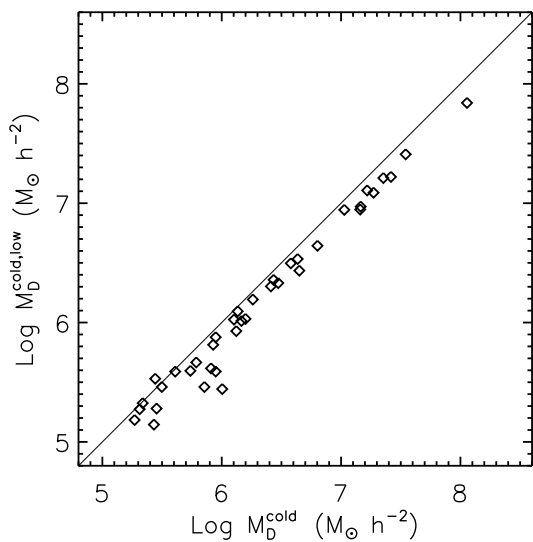
Fig. 3.— The correlation between the mass of the "cold dust" component obtained from fitting two modified black-body functions to the 60, 100 and $170\,\mu$m flux densities versus the mass of the "cold dust" component in the lower limit case, obtained from fitting a single modified black-body function to the 100 and $170\,\mu$m flux densities. The solid line represents the unit slope zero offset line.
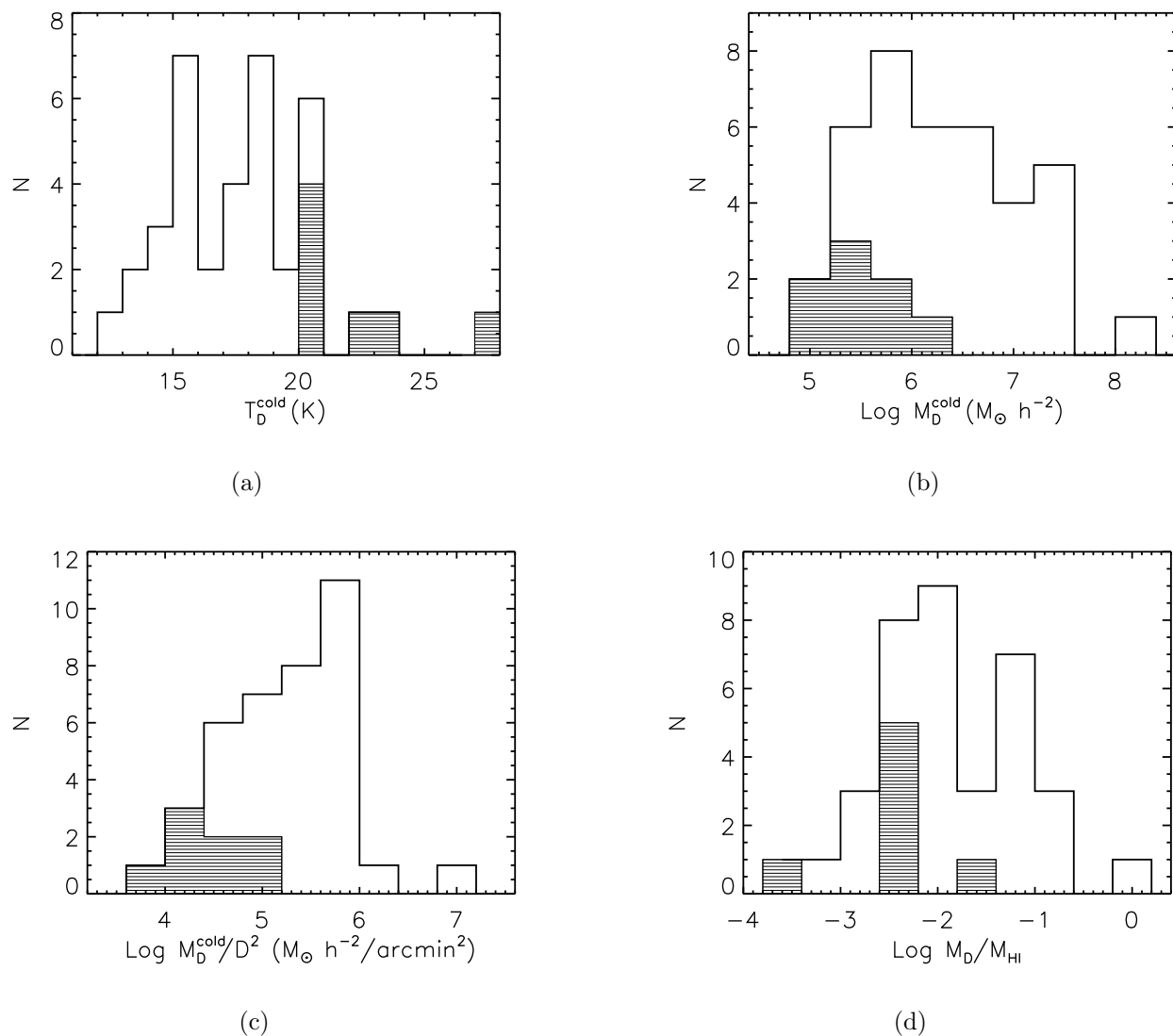
Fig. 4.— The distribution of a) cold dust temperatures; b) cold dust masses; c) cold dust mass surface densities; d) dust-to-HI mass ratio. The hatched histograms represent the distributions for the "one component" galaxies. The galaxy with the warmest dust temperature, $T_D = 34.7$ K, was excluded from the histogram for display reasons only.
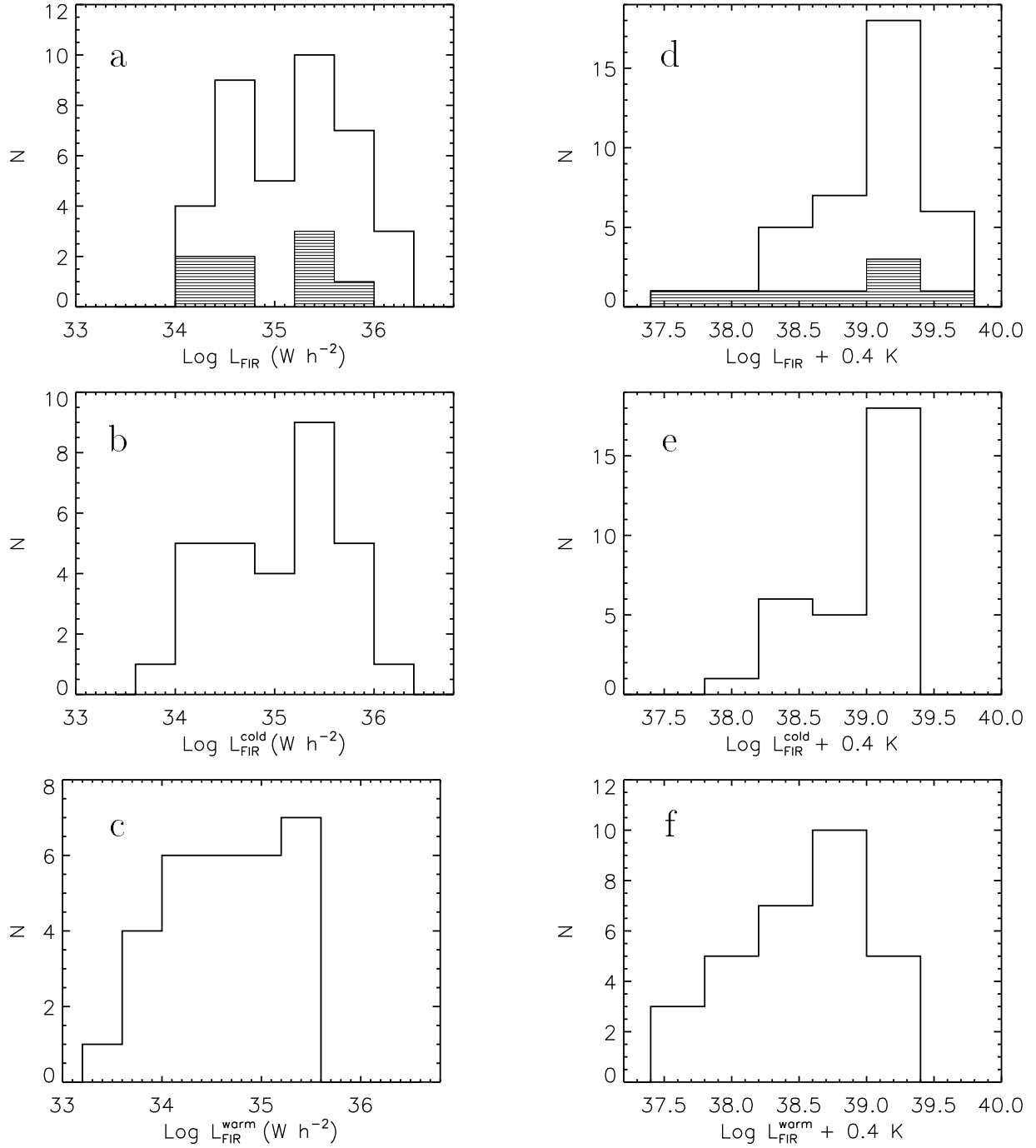
Fig. 5.— The distribution of a) FIR luminosities; b) FIR luminosities of the cold dust component; c) FIR luminosities of the warm dust component; d) normalized FIR luminosities (to the K′ band magnitude) ; e) normalized FIR luminosities of the cold dust component; f) normalized FIR luminosities of the warm dust component. The hatched histograms represent the distributions for the "one component" galaxies.
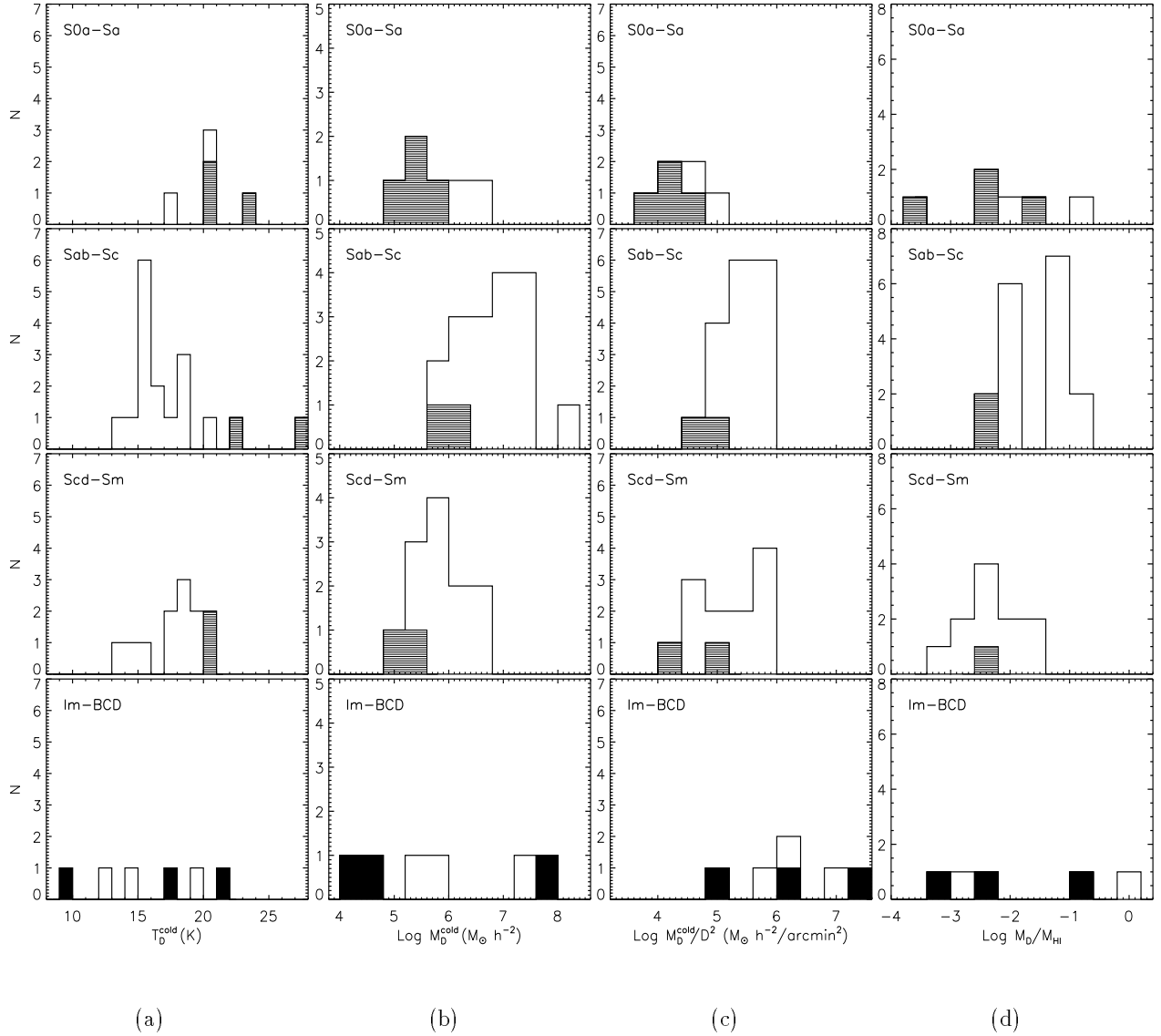
Fig. 6.— The distribution of a) cold dust temperatures $T_{\mathrm{D}}^{\mathrm{cold}}$; b) cold dust masses $M_{\mathrm{D}}^{\mathrm{cold}}$; c) cold dust mass surface densities $M_{\mathrm{D}}^{\mathrm{cold}}/D^2$; d) dust-to-HI mass ratio for different Hubble types. The hatched histograms represent the distributions for the "one component" galaxies. The filled histograms represent the distributions for the galaxies with detections only at two wavelengths (100 and 170 μm). For the latter cases the dust temperatures are only upper limits and the dust masses are only lower limits. The galaxy with the warmest dust temperature, 33.4 K, is not plotted in the histogram (panel a, for S0a-Sa) for display reasons only.
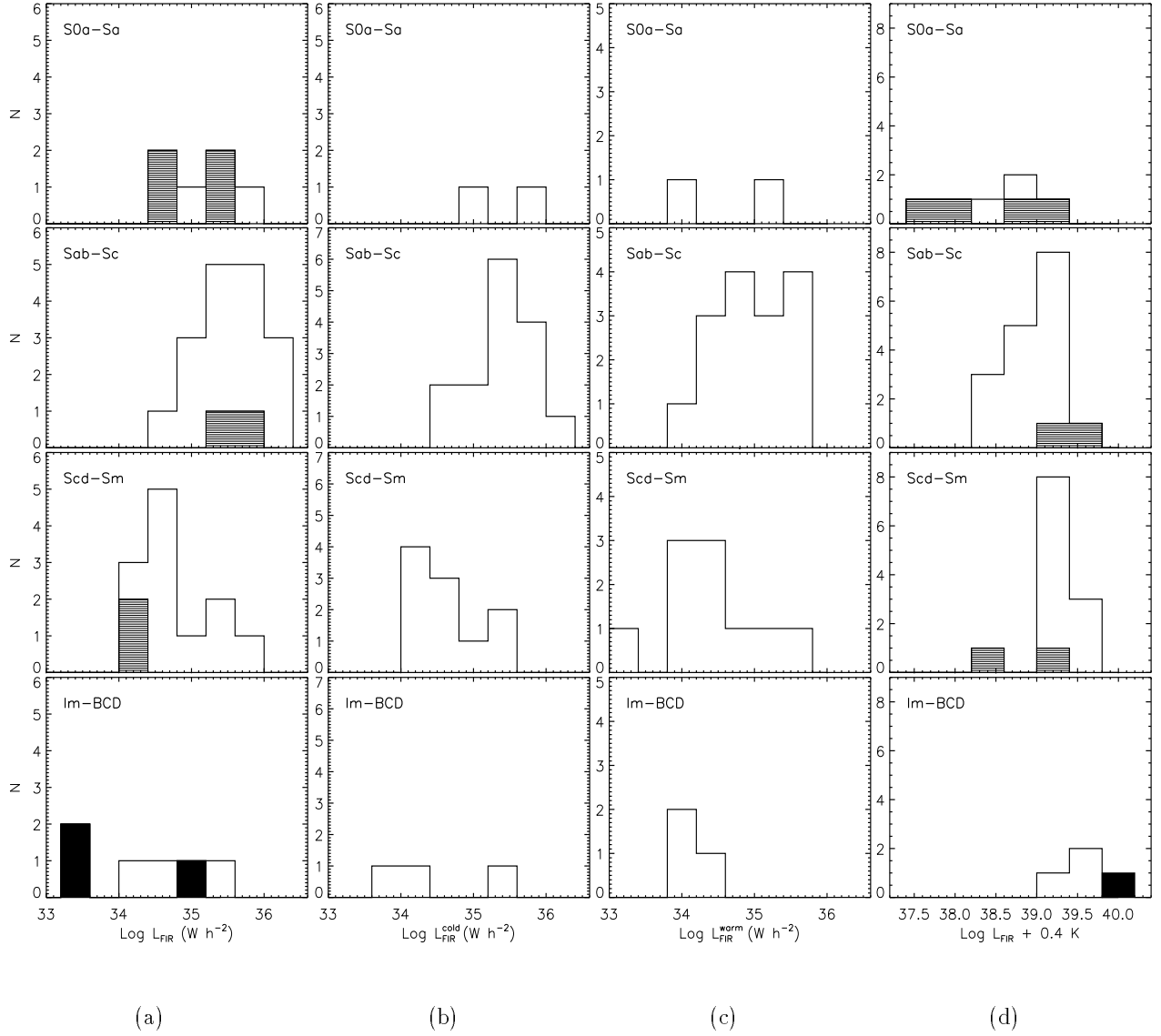
Fig. 7.— The distribution of: a) FIR luminosity; b) FIR luminosity of the cold component; c) FIR luminosity of the warm component; d) normalized FIR luminosity (to the K′ band magnitude) for different Hubble types. The hatched histograms represent the distributions for the "one component" galaxies. The filled histograms represent the distributions for the galaxies (all BCDs) with detections only at two wavelengths (100 and 170 μm). From these, two BCDs don't have available K′-band magnitudes and therefore they are excluded from the histogram (panel d, for Im-BCD).
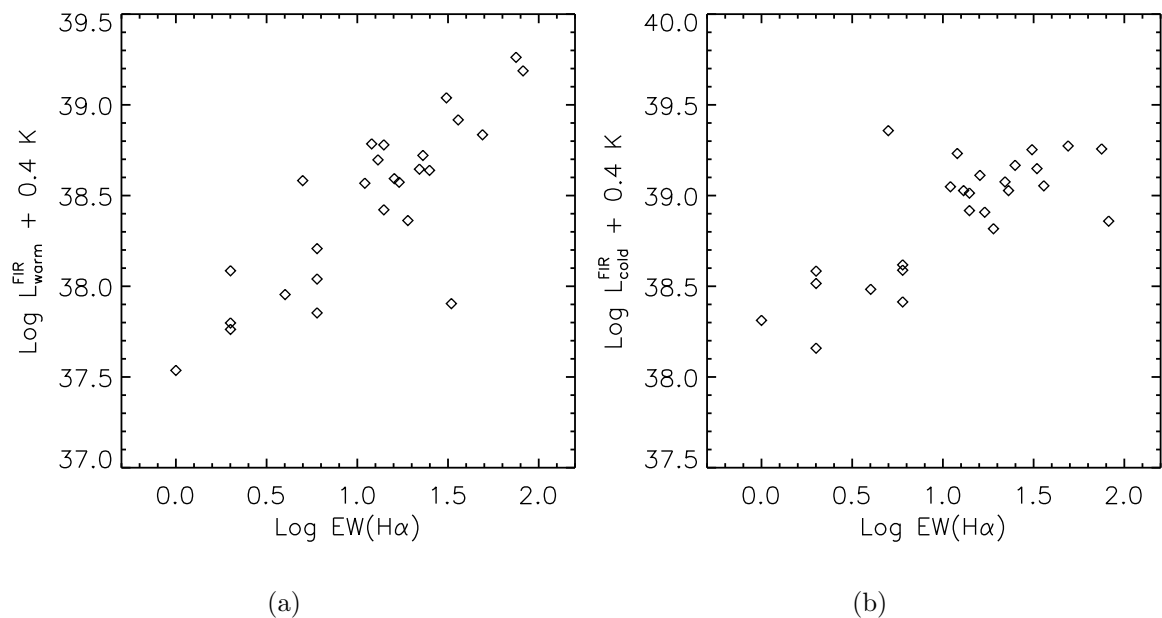
Fig. 8.— a) The normalized FIR luminosities of the warm dust component (normalized to the K' band magnitudes) versus the Hα equivalent widths. b) The same for the cold dust component.
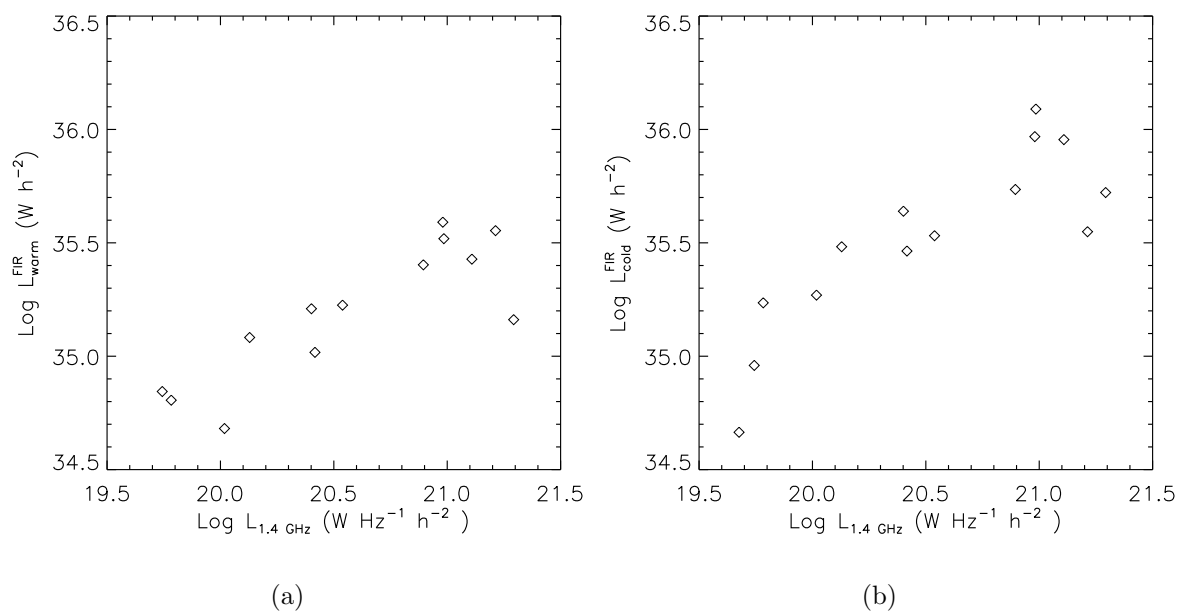
Fig. 9.— a) The warm FIR-radio correlation. b) The cold FIR-radio correlation.

Table 2. Results from constrained fits of two modified black-bodies to the 60, 100 and 170 μm flux densities

VCC	$M_{\rm D}^{\rm warm}$ $M_\odot \times h^{-2(1)}$ $\times 10^2$	$M_{\rm D}^{\rm cold}$ $M_\odot \times h^{-2}$ $\times 10^5$	$T_{\rm D}^{\rm cold}$ K	$\sigma(T_{\rm D}^{\rm cold})^{(2)}$ K	$M_{\rm D}/M_{\rm HI}{}^{(3)}$	$L_{\rm FIR}$ $W \times h^{-2}$ $\times 10^{34}$	$L_{\rm FIR}^{\rm cold}$ $W \times h^{-2}$ $\times 10^{34}$	note[4]
1	4.9	7.2	14.1	1.3	$\cdots$	1.6	0.95	
66	120.	140.	15.5	0.4	0.0067	51.	34.	
87	4.9	8.9	14.0	1.0	0.0082	1.8	1.1	
92	230.	1100.	13.6	0.2	0.0459	160.	120.	
152	73.	43.	18.5	0.5	0.0221	40.	29.	
318	6.1	16.	14.9	0.5	0.0040	3.8	2.9	
459	4.8	1.9	19.7	0.9	0.0024	2.5	1.9	
460	110.	38.	20.2	0.9	0.0087	60.	44.	
655	20.	260.	12.6	0.2	0.6379	20.	17.	
664	38.	10.	15.7	2.5	0.0092	7.9	2.5	
692	25.	63.	14.9	0.8	0.0513	16.	12.	
836	$\cdots$	$\cdots$	$\cdots$	$\cdots$	$\cdots$	$\cdots$	$\cdots$	see Table 3
857	28.	110.	15.4	0.3	0.0483	28.	24.	
873	180.	190.	16.1	0.2	0.0832	80.	54.	
912	28.	8.9	20.5	1.2	0.0087	15.	11.	
971	12.	8.5	17.8	0.5	0.0016	6.3	4.6	
1002	33.	27.	18.5	0.5	0.0110	23.	19.	
1003	$\cdots$	$\cdots$	$\cdots$	$\cdots$	$\cdots$	$\cdots$	$\cdots$	see Table 3
1043	100.	170.	16.3	0.3	0.0906	67.	53.	
1110	86.	150.	15.2	0.4	0.0711	43.	30.	
1189	8.3	15.	15.6	0.3	0.0103	4.8	3.6	
1253	$\cdots$	$\cdots$	$\cdots$	$\cdots$	$\cdots$	$\cdots$	$\cdots$	see Table 3
1326	$\cdots$	$\cdots$	$\cdots$	$\cdots$	$\cdots$	$\cdots$	$\cdots$	see Table 3
1379	45.	26.	18.4	0.5	0.0068	24.	17.	
1410	10.	8.1	15.7	0.7	0.0085	3.5	2.0	
1419	$\cdots$	$\cdots$	$\cdots$	$\cdots$	$\cdots$	$\cdots$	$\cdots$	see Table 3
1450	$\cdots$	$\cdots$	$\cdots$	$\cdots$	$\cdots$	$\cdots$	$\cdots$	see Table 3
1552	11.	13.	17.7	0.6	0.1446	8.1	6.5	
1554	250.	45.	19.0	0.5	0.0030	71.	35.	
1575	49.	13.	18.5	1.3	0.0317	16.	9.1	

Table 2—Continued

VCC	$M_\mathrm{D}^\mathrm{warm}$ $\mathrm{M_\odot \times h^{-2}}^{(1)}$ $\times 10^2$	$M_\mathrm{D}^\mathrm{cold}$ $\mathrm{M_\odot \times h^{-2}}$ $\times 10^5$	$T_\mathrm{D}^\mathrm{cold}$ K	$\sigma(T_\mathrm{D}^\mathrm{cold})^{(2)}$ K	$M_\mathrm{D}/M_\mathrm{HI}^{(3)}$	L_FIR $\mathrm{W\times h^{-2}}$ $\times 10^{34}$	$L_\mathrm{FIR}^\mathrm{cold}$ $\mathrm{W\times h^{-2}}$ $\times 10^{34}$	note$^{(4)}$
1678	1.7	3.1	19.0	1.5	0.0006	2.8	2.5	
1686	18.	6.1	19.3	0.8	0.0030	7.9	5.4	
1690	270.	230.	17.0	0.3	0.0745	130.	93.	
1699	13.	2.7	17.9	0.9	0.0012	3.3	1.5	
1725	$\cdots$	$\cdots$	$\cdots$	$\cdots$	$\cdots$	$\cdots$	$\cdots$	see Table 3
1727	190.	350.	15.8	0.3	0.1144	120.	90.	
1730	64.	30.	18.2	0.9	0.1134	28.	18.	
1757	$\cdots$	$\cdots$	$\cdots$	$\cdots$	$\cdots$	$\cdots$	$\cdots$	see Table 3

$^{(1)}$h = H$_0$/100 and H$_0$ is the Hubble constant.

$^{(2)}$The uncertainty in the temperature of the cold dust component.

$^{(3)}$The dust-to-HI-gas mass ratio.

$^{(4)}$In eight cases there was no evidence for two dust components with different temperatures. For these galaxies there is a note that sends the reader to Table 3, where these galaxies are listed.

Table 3.   Results from one modified black-body fit to the 60, 100 and 170 μm flux densities

(1) VCC	(2) M_D $M_\odot \times h^{-2}$ $\times 10^4$	(3) T_D K	(4) $\sigma(T_D)$ K	(5) M_D/M_{HI}	(6) L_{FIR} $W \times h^{-2}$ $\times 10^{34}$
130[a]	2.2	21.4	3.0	0.0007	0.37
836	120.	27.1	0.3	0.0052	83.
848[a]	10000.	9.0	0.5	0.2026	9.1
1003	55.	23.9	0.2	0.0061	17.
1253	36.	20.6	0.8	0.0051	4.7
1326	7.2	34.7	1.2	0.0004	20.
1419	14.	20.4	1.4	$\cdots$	1.7
1450	92.	22.1	0.3	0.0063	18.
1725	17.	20.1	0.7	0.0026	1.9
1750[a]	5.1	17.8	1.9	0.0050	0.27
1757	28.	20.1	0.3	0.0282	3.0

[a]VCC 130/848/1750 have detections only at 100 and 170 μm and therefore their dust masses represent lower limits and their dust temperatures upper limits.